

Turbulent spots in an oscillatory flow over a rough wall

M. Mazzuoli * G. Vittori †

May 13, 2019

Abstract

We describe the results of a direct numerical simulation inspired by laboratory experiments [S. Carstensen and B. M. Sumer and J. Fredsøe “A note on turbulent spots over a rough bed in wave boundary layers”, *Physics of Fluids*, **24**, 2012], which showed the formation of turbulent spots in an oscillatory boundary layer over a rough wall. Even though, differently from the experiments, the wall we consider is characterized by a regular roughness, turbulent spots with similar characteristics are observed. The numerical results provide information on transition to turbulence and on the early stages of formation of the turbulent spots. In particular, the formation of low-speed streaks and the subsequent generation of turbulent spots are described. The speed of the extreme points of the spots is obtained from the numerical results. Moreover, the effects of the wall roughness on the speed of the turbulent spots are discussed.

1 Introduction

Since Emmons [1951] observed the formation of turbulent spots in a steady boundary layer over a smooth wall, many investigations have been devoted to the study of these constituents of transitional flows, due to their role in the inception of turbulence. Turbulent spots are isolated regions of random velocity fluctuations superposed to a laminar flow and appear at random positions in the vicinity of the wall when the Reynolds number exceeds a critical value. Most of the research on turbulent spots considers steady flows even though oscillatory flows are present in many industrial applications, natural environments and biological flows. For example, an oscillatory boundary layer develops at the sea bottom under sea waves. Only recently, attempts

*Department of Civil, Chemical and Environmental Engineering, University of Genoa, Via Montallegro 1, 16145 Genoa, ITALY

†Department of Civil, Chemical and Environmental Engineering, University of Genoa, Via Montallegro 1, 16145 Genoa, ITALY

to study both experimentally and numerically the formation and the characteristics of turbulent spots in an oscillatory boundary layer over a smooth wall were made by Carstensen et al. [2010] and by Mazzuoli et al. [2011a]. It was observed that turbulent spots appear for values of the Reynolds number such that the flow is in the intermittently turbulent regime. Indeed, the flow regime in the oscillatory boundary layer over a smooth wall can be laminar, disturbed laminar, intermittently turbulent or fully turbulent, depending on the value of the Reynolds number R_δ [Vittori and Verzicco, 1998]. Herein, the Reynolds number R_δ is defined with the amplitude U_0 of the velocity oscillations outside the boundary layer, the viscous length δ and the kinematic viscosity ν of the fluid. The viscous length δ is equal to $\sqrt{\nu T/\pi}$, where T is the period of the fluid oscillations.

The formation of turbulent spots over a smooth wall in an oscillatory boundary layer was first observed by Carstensen et al. [2010] during accurate laboratory experiments. During the transition process from the laminar to the turbulent regime, which takes place every oscillation cycle, Carstensen et al. [2010] observed different coherent vortex structures, namely vortex tubes and turbulent spots. Vortex tubes are two-dimensional horizontal vortices, with the axes in the span-wise direction, that were observed for R_δ ranging from 374 to 775. For R_δ larger than 548 and after the outer velocity has reached its maximum, Carstensen et al. [2010] observed also the formation of turbulent spots. The direct numerical simulations by Mazzuoli et al. [2011a] reproduced two of the experiments by Carstensen et al. [2010]. In the simulations by Mazzuoli et al. [2011a] and by Mazzuoli et al. [2011b], turbulent spots appeared near the end of the accelerating phases and some of them had the characteristic arrow-head shape, typical of the spots that form in steady boundary layers. Mazzuoli et al. [2011a] also determined some of the characteristics of the turbulent spots that are difficult to measure during laboratory experiments. In particular, Mazzuoli et al. [2011a] measured the speed of the head and tail of the turbulent spots for different values of R_δ and obtained values of the ratio between the speeds of the head (tail) of the turbulent spots and that of the free stream velocity that are similar to those of the turbulent spots forming in steady boundary layers [Schubauer and Klebanoff, 1955].

Carstensen et al. [2012] continued their investigation on the formation of turbulent spots in oscillatory boundary layers and considered a rough wall, made up with well-sorted sand grains. They made ten flow visualizations for values of R_δ ranging from 316 to 447 and observed that turbulent spots formed for values of R_δ smaller than the critical value for the formation of turbulent spots in the smooth-wall case. Similarly to the smooth wall case, the phase at which turbulent spots appeared decreased as R_δ was increased. Moreover, the speed of the leading edge, they measured, was smaller than that of turbulent spots forming over a smooth wall. Direct numerical simulations of an oscillatory flow over a rough wall were conducted by Fornarelli

and Vittori [2009], Mazzuoli and Vittori [2016] and Ghodke and Apte [2016] who considered rough walls made up with elements arranged in a regular pattern. The roughness elements were half spheres with diameter equal to 6.95δ in Fornarelli and Vittori [2009] and full spheres with diameter equal to 6.95δ and 2.32δ in Mazzuoli and Vittori [2016] and equal to 6.95δ in Ghodke and Apte [2016]. In all cases the roughness elements were arranged in a hexagonal pattern. These studies provided detailed information on the flow dynamics. Mazzuoli and Vittori [2016] described the dynamics of the vortex structures which appear close to the wall and were able to identify three flow regimes: the laminar, the transitional turbulent and the hydrodynamically rough turbulent regimes. The value of the Reynolds number and the size of the roughness determine the flow regime. In the hydrodynamically rough turbulent regime, turbulent fluctuations grow at phases when the external velocity reaches its largest values. In the transitional turbulent regime, that Mazzuoli and Vittori [2016] observed only for the wall with the smallest roughness elements and for the largest values of R_δ , turbulent fluctuations appeared during the decelerating phases of the oscillatory cycle. The results by Ghodke and Apte [2016] showed the formation of horseshoe vortex structures close to the roughness elements which later underwent distortion and breaking. Contrary to the steady flow over a rough bed, Ghodke and Apte [2016] showed that bed-induced production terms are significant and comparable to the shear production terms.

The direct numerical simulations by Fornarelli and Vittori [2009], Ghodke and Apte [2016] and Mazzuoli and Vittori [2016] could not reproduce turbulent spots because of the limited size of the computational domain they used. In the present contribution, a direct numerical simulation of the oscillatory flow over a rough wall is performed, considering a computational domain with a size large enough to detect the formation of turbulent spots. The aim of the investigation is to reproduce numerically the formation of turbulent spots for conditions similar to those of Carstensen et al. [2012], that first showed the formation of turbulent spots in an oscillatory boundary layer in the rough wall case. Moreover, we investigate the transition mechanism that gives rise to turbulent spots and measure the velocity of the extreme points of the spots.

In the next section we introduce the problem and briefly describe the numerical approach. Then, we describe the numerical procedure we use to detect and measure the characteristics of the turbulent spots and we discuss the results. The last section is devoted to the conclusions.

2 The numerical model

We consider a fluid of constant density ρ , bounded by a horizontal rough wall. The wall we consider is made up of spheres lying on a flat surface

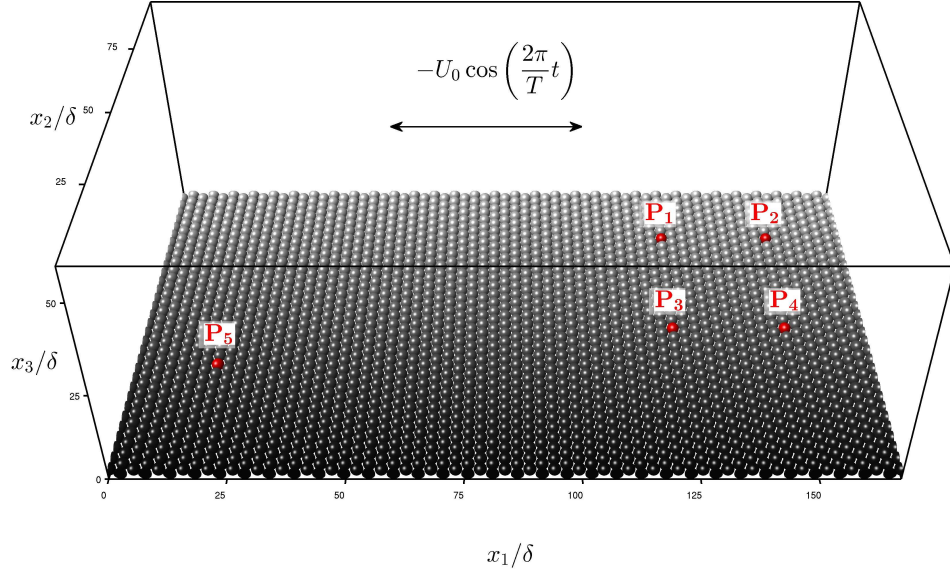


Figure 1: Sketch of the problem. The velocity of the flow far from the rough wall oscillates with period T ($U_e = -U_0 \cos(2\pi t/T)$). Measuring probes are located at: $P_1 = (122.83\delta, 3.16\delta, 77.65\delta)$; $P_2 = (148.96\delta, 3.16\delta, 77.65\delta)$; $P_3 = (122.83\delta, 3.16\delta, 44.80\delta)$; $P_4 = (122.83\delta, 3.16\delta, 44.80\delta)$; $P_5 = (18.29\delta, 3.16\delta, 32.85\delta)$;

and arranged in a hexagonal pattern (see Fig. 1). The flow is driven by the oscillating pressure gradient:

$$\frac{\partial p}{\partial x_1} = -\rho U_0 \frac{2\pi}{T} \sin\left(\frac{2\pi t}{T}\right), \quad (1)$$

which is referred to a right-handed Cartesian coordinate system with the x_1 -axis in the direction of the fluid oscillations and the x_3 -axis vertical and pointing upward (see Fig.1). The fluid far from the wall oscillates uniformly with velocity $U_e(t) = -U_0 \cos(2\pi t/T)$. The flow field is determined by numerically solving the incompressible Navier-Stokes equations with a second-order fractional-step method. The temporal discretization is semi-implicit. The viscous term is approximated with the Crank-Nicolson scheme and a low storage three-step Runge-Kutta approach is used for the nonlinear term. The spatial derivatives are evaluated by central finite-differences on a staggered, uniform and equispaced grid. No-slip condition at the surface of the roughness elements (spheres) is forced by means of a variant of the immersed boundary method proposed by Uhlmann [2005]. The code underwent a long validation and was used for solving problems similar to

the present one [e.g. Mazzuoli and Uhlmann, 2017]. In the present investigation we consider spheres with diameter D equal to 5 mm. Carstensen et al. [2012] used a rough wall made by glueing to a plane wall a single layer of sand with a mean grain size equal to 2.5 mm and Nikuradse’s equivalent roughness equal to 5 mm. Under steady flow conditions and on a bed made with spheres of diameter d , arranged with the densest packing, experimental and numerical studies [Schlichting and Gersten, 2016, Singh et al., 2007, Detert et al., 2010, Pimenta et al., 1975, Ligrani and Moffat, 1986] suggest values of the equivalent sand roughness ranging from $0.62 d$ to $0.81 d$. However, no information is available for oscillatory flows at moderate values of the Reynolds number, *which recover laminar regime during part of the oscillating cycle*. To allow a comparison of the present results with the experimental measurements by Carstensen et al. [2012], we assume that Nikuradse’s sand-roughness of the present geometry is similar to that of the experiments by Carstensen et al. [2012] (D). However, it should be kept in mind that that the present geometry is different from that of the experimental measurements by Carstensen et al. [2012], that were made considering an irregular roughness (natural sand). For the value of δ equal to that of the experiment by Carstensen et al. [2012], the value of D we chose corresponds to 2.8δ . In the experiments by Carstensen et al. [2012] the maximum free stream velocity, and consequently R_δ , increased from half cycle to half-cycle, while in the present simulations R_δ is fixed. Preliminary runs carried out for $R_\delta = 200$ and 300 , did not show the development of turbulent spots. The value of R_δ of the numerical simulation that showed the formation of turbulent spots, which is equal to 400 , is the same as that of the experiment shown in figure 4 by Carstensen et al. [2012]. In order to allow for the formation of turbulent spots, a domain of size 167.25δ , 95.57δ and 59.73δ in the stream-wise, span-wise and cross-stream directions is used. The rough wall consists of 32 rows composed of 64 spheres each. The number of computational points $N_{x1} \times N_{x2} \times N_{x3}$ is equal to $3584 \times 2048 \times 1280$. The size of the computational domain is comparable to that of the area shown in Fig. 1 by Carstensen et al. [2012]. Moreover, 61 computational points are distributed along the diameter of each sphere, resulting in a total of 11310 computational points over its surface, which appears sufficient for an accurate modeling. Finally, the time-step is constant, with 61875 steps per oscillation cycle. To speed up the attainment of a steady state, the initial velocity field is that of the Stokes flow over a plane wall at $x_3 = 0$. The first oscillation cycle is discarded because it is affected by initial conditions.

3 Results

The experimental visualizations by Carstensen et al. [2012] suggest that turbulent spots should appear when the free stream velocity is maximum. The

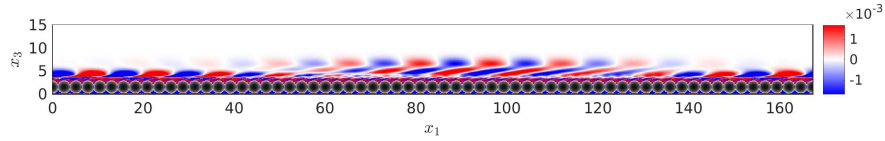


Figure 2: Spanwise fluctuating vorticity component, divided by U_0/δ and averaged in the spanwise direction at $t=1.5 T$.

present numerical simulation shows that the first oscillation cycle is in the laminar regime. During the second cycle, at the end of the accelerating phases, only vortex tubes with spanwise axes are *observed* (see Fig. 2). The vortex tubes are nearly equispaced with an average spacing of 13.75δ , similar to that of the vortex tubes which form over a smooth wall [Blondeaux and Vittori, 1994, Vittori and Verzicco, 1998, Costamagna et al., 2003]. In the decelerating phases of the cycle, the vortex tubes decrease in intensity because of viscous effects. At the end of the 5th half cycle, vortex tubes form and subsequently bend and break, originating smaller vortices which dissipate because of viscous effects. Figure 3 shows the vortex tubes during the decelerating phase of the 6th half oscillation cycle ($t = 2.62T$). In the central part of the figure, the vortex tubes are two-dimensional while close to the streamwise boundaries they undergo a three-dimensional instability. The spanwise wavelength of the three-dimensional unstable modes is a sub-multiple of the width of the computational domain, as could be expected. However, such wavelength is small compared to the spanwise dimension of the computational domain. The presence of random velocity components, associated with the natural transition, can be observed in Fig.3 (blue and yellow surfaces). The natural transition takes place only during the central part of the 3rd oscillation cycle. During the late decelerating phase of the 6th half-cycle, the flow tends to recover the laminar regime but weak regions of residual random vorticity are present far from the wall. Turbulent spots form for the first time during the accelerating phase of the 6th half cycle, but they are weak. For this reason the data we post-processed to obtain quantitative information on turbulent spots, refer to the 7th half cycle. The first stages of development of a turbulent spot can be seen in Fig. 4, which illustrates the time development of the flow during the 7th half cycle. During the last part of the accelerating phases, no intense turbulent fluctuations are observed close to the wall and streaks elongated in the stream-wise direction appear (Figs. 4a). As time progresses in the accelerating phase, the streaks grow in intensity while the small vortex structures, which survive from the previous half-cycle, also gain strength because of the strain associated with the mean flow. Residual vortex structures (see Fig. 5 and Movie 1), which are convected by the fluid, provide a localized instantaneous disturbance which destabilizes the streaks and triggers the following

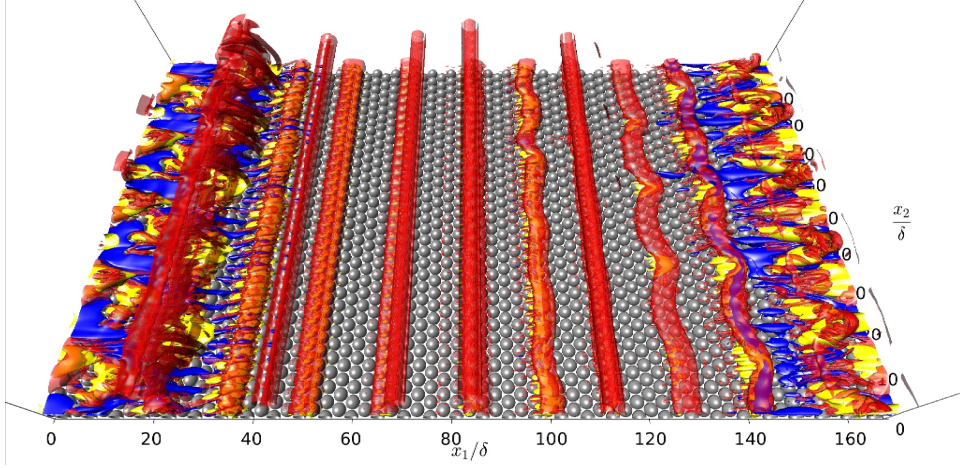


Figure 3: Instability of the vortex tubes $t=2.62 T$. Isocontours of u'_1 ($u'_1 = 0.1 U_0$, blue, $u'_1 = -0.1 U_0$, yellow) and isosurfaces of λ_2 , defined by Jeong and Hussain [1995] (red surfaces - $\lambda_2 = -0.001 U_0^2 / \delta^2$).

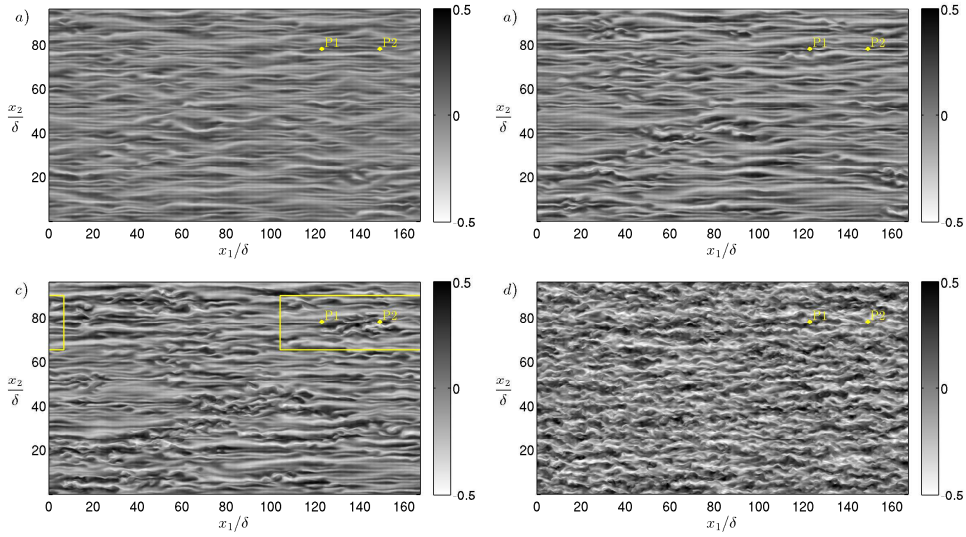


Figure 4: Fluctuating streamwise velocity component (u'_1) in the plane $x_3 = 3.2\delta$. a) $t= 3.37T$, b) $t= 3.40T$, c) $t= 3.43T$, d) $t= 3.5T$. The complete time development can be seen in Movie 2 (supplementary material).

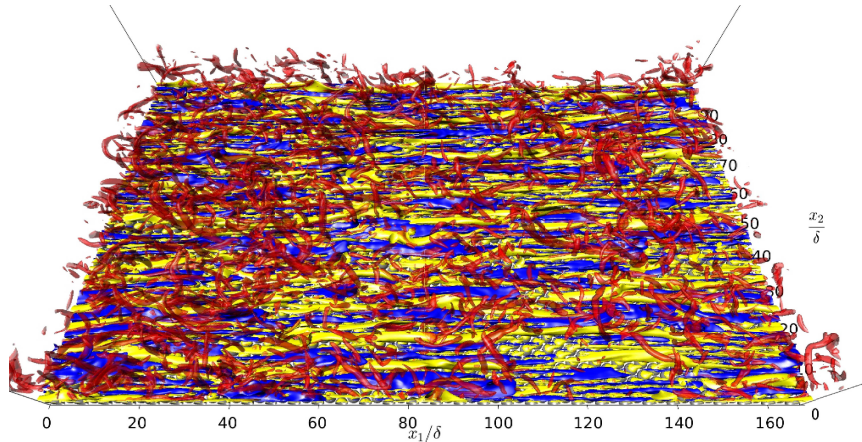


Figure 5: Interaction of low and high speed streaks with residual turbulent structures at $t=3.42T$. Low and high speed streaks are visualized by isosurfaces of u'_1 ($u'_1 = 0.1 U_0$, blue, $u'_1 = -0.1 U_0$, yellow) while the isosurfaces of λ_2 , defined by Jeong and Hussain [1995], ($\lambda_2 = -0.01 U_0^2 / \delta^2$, red) show the decaying vortex structures generated during the previous half-cycle.

rapid transformation of the streaks into turbulent spots (see Figs. 4b,c). At the end of the accelerating phase, small scale eddies occupy the region close to the wall and no turbulent spot can be distinguished (see Fig 4d). As shown in Figs. 4b,c, several turbulent spots appear simultaneously at random positions. After their birth, turbulent spots grow in intensity and size, and eventually merge. At the beginning of the decelerating phases, the turbulent regime develops in the whole (x_1, x_2) -plane. During the last part of the decelerating phases, turbulent vortex structures damp out and the flow tends to relaminarize. In the following half cycles the process of generation of turbulent spots and subsequent relaminarization of the flow repeats similarly. It thus appears that, starting from the last part of the 6th half cycle, the flow is subject to a by-pass transition mechanism, followed by a relaminarization phase, during each half cycle. The process that gives rise to the turbulent spots is very rapid, as witnessed by Fig. 4 which shows the evolution of the flow field in a time interval equal to 0.08π (4% of the oscillation period). Since the present flow is in the transitional turbulent regime, that has some analogies with the transitional regime over a smooth wall [Mazzuoli and Vittori, 2016], on the basis of the smooth wall results [Mazzuoli et al., 2011a], it is reasonable to expect that the process of formation of turbulent spots would be slower (faster) than that presently observed, if a value of the Reynolds number smaller (larger) than the present one was considered. Movies 1 and 2, provided as supplementary material, show the formation of several turbulent spots during the 4th cycle.

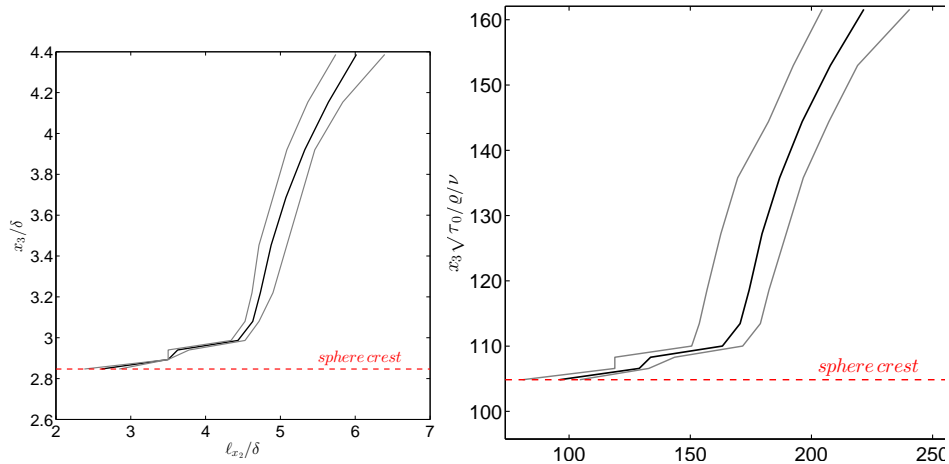


Figure 6: Vertical profile of twice the streamwise-averaged separation distance at which the value of the span-wise spatial correlation of u'_1 is minimum, scaled with δ (left panel) and with $\nu/\sqrt{\overline{\tau}_0/\rho}$ (right panel). In the right panel, the distances in the right vertical axis are measured from the position of a theoretical wall defined by Carstensen et al. [2012] and located at $x_3/\delta=0.85 D/\delta$. The spacing is computed at different phases in the cycle between $t=3.455T$ and $t=3.55 T$. The two broken lines indicate the maximum and minimum values obtained in the considered time interval.

Fig. 6 shows twice the average, in the stream-wise direction, of the separation distance, ℓ_{x_2} , at which the value of the span-wise spatial correlation of u'_1 reaches the absolute minimum. It is worthwhile to mention that the value of ℓ_{x_2} provides an estimate of the averaged spanwise spacing between two adjacent high-speed streaks. The value of ℓ_{x_2} depends on the distance from the wall and increases rapidly in a region of order δ moving away from the top of the spheres, which is located at $x_3/\delta=2.8$. In particular at $x_3/\delta = 3$, ℓ_{x_2} is approximately equal to 4.5δ . The right panel of Fig. 6 shows the same quantity as the left panel, divided by $\nu/\sqrt{\overline{\tau}_0/\rho}$. The bottom shear stress τ_0 has been computed as the total stress at the distance from the spheres where the viscous stress is maximum. Since τ_0 varies with time, we use the time-averaged value of τ_0 in the considered interval ($\overline{\tau}_0$). It can be seen in Fig. 6 that the spacing of the streaks in the viscous region close to the crests is of the order of $100 \nu/\sqrt{\overline{\tau}_0/\rho}$.

The fluctuating components of the flow field are computed with respect to values averaged over planes characterized by a constant value of x_3 . The correct spatial average operator should exploit the periodicity of the roughness pattern, as discussed in Mazzuoli and Vittori [2016]. Such procedure allows to filter out the random fluctuations from those due to the deterministic vortex structures which form on the surface of each roughness element. However, the latter procedure is burdensome and preliminary tests showed

that the values of the speeds of the extreme points of one spot obtained by considering both procedures, are within the accuracy of the computed values.

Carstensen et al. [2012] detected the presence of turbulent spots from the output of either velocity or bottom shear stress probes, because the presence of a turbulent spot causes the measuring instrument to record large random fluctuations. Fig. 7 shows the output of three numerical probes that record streamwise velocity (u_1) and pressure fluctuations (p') at the points P_1 , P_2 and P_5 shown in Fig. 1. The points P_1 , P_2 and P_5 are at positions where a turbulent spot appears during the considered time interval, even though at point P_5 turbulence develops slightly later. The passage of a turbulent spot can be evinced from the large amplitude fluctuations recorded by the probes P_1 and P_2 , when the external velocity (blue line) is going to attain its maximum. Probe P_5 shows fluctuations at later times because not all turbulent spots appear simultaneously. Eventually the spots merge and turbulent fluctuations develop in the whole boundary layer.

A first estimate of the speed of propagation of the turbulent spot can be obtained by computing the time interval at which the cross correlation between p' (or u'_1), measured at two longitudinal positions, attains the first maximum value. According to this procedure, the average velocity of the spot that propagates from the point P_1 to the point P_2 is $0.83 U_0$. A further measurement made considering the points P_3 and P_4 , positioned as shown in Fig. 1, gives $0.60 U_0$, thus showing the variability of the velocity of the spots.

A more accurate evaluation of the evolution of the turbulent spots can be gained by measuring the speed of the head, tail and lateral points (sides). The speed of the extreme points is evaluated by following their position in time. Following Mazzuoli et al. [2011a], turbulent spots are detected considering the production term of turbulent kinetic energy (TKEP) in the turbulent kinetic energy (TKE) equation. Similarly to Mazzuoli et al. [2011a] we made preliminary tests and considered different turbulent quantities to detect the extreme points of a turbulent spot (λ_2 defined by Jeong and Hussain [1995], TKE and the absolute values of the fluctuating velocity components) and obtained similar values of the velocity of the head and tail of the turbulent spot (see Fig. 8). The identification of the extreme points of the spot is carried out by considering a rectangular region which contains the spot (see the yellow box in Fig. 4). The size and position of the box is selected in such a way that the rectangle be simultaneously large enough to contain the spot and small enough to contain only the spot of interest. The horizontal plane selected for the measurements is the plane where the value of the TKE is maximum. During the evolution of the spots, the position of the maximum of the TKE is, with a good approximation, constant and equal to $x_3 = 3.2\delta$; therefore the measurements are carried out considering the plane $x_3 = 3.2\delta$. The x_1 -coordinates of the head and tail of the spot

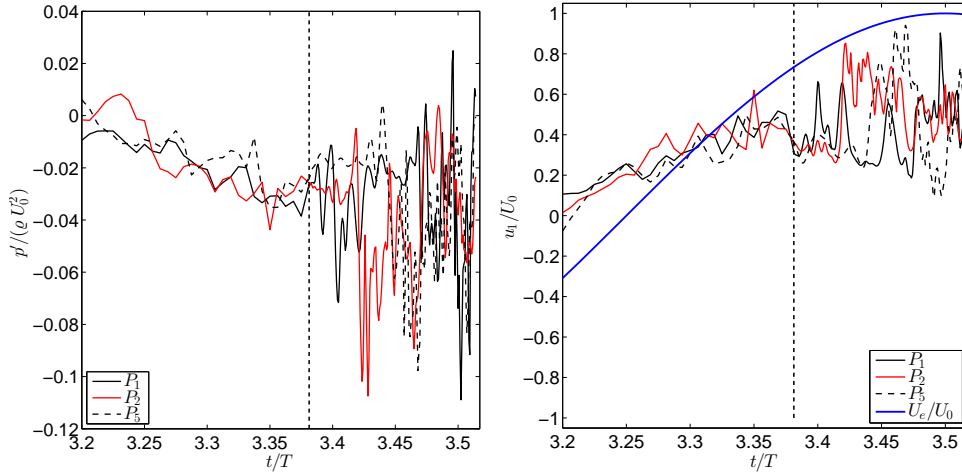


Figure 7: Time development of the fluctuating component of pressure p' (left panel) and of the streamwise velocity component (right panel) at the three measuring points shown in Fig. 1. The outer velocity is shown in the right panel with a thick blue line. The frequency of acquisitions is larger on the right-hand side of the vertical dashed line.

are taken as the values of x_1 such that the quantity

$$\mathcal{T}_1(x_1) = \frac{1}{x_2^B - x_2^A} \int_{x_2^A}^{x_2^B} \text{TKEP}(x_1, x_2) dx_2 \quad (2)$$

exceeds a threshold value. Similarly, the positions of the left and right extremes of the spot are determined by defining the function $\mathcal{T}_2(x_2)$. Then, the speed of the extreme points of a spot is evaluated as the slope of the corresponding line in the $(t, x_{1,2})$ -plane.

The accuracy of the procedure is affected by different elements. The first element is the contribution of the small turbulence structures to $\mathcal{T}_1(x_1)$. Such small structures do not belong to the spot but, as the spot grows in size, emerge inside the chosen rectangular region and influence the TKEP. The second element, that affects directly the evaluation of the speed of the extreme points, is related to the time interval during which the position of the extreme points is evaluated. We estimate that the described procedure provides values of the speed of the extreme points of the spots with an accuracy of 10%.

The head, tail and lateral points (extreme points) of the spots travel at different speeds. During the early stages of the development, the velocity of the head and tail is approximately constant, as proven by Fig. 8, which shows the position of the head and tail of one turbulent spot versus time. The quantities averaged over the measurements made on 6 spots are presented and discussed herein. The averaged velocities of the extreme points

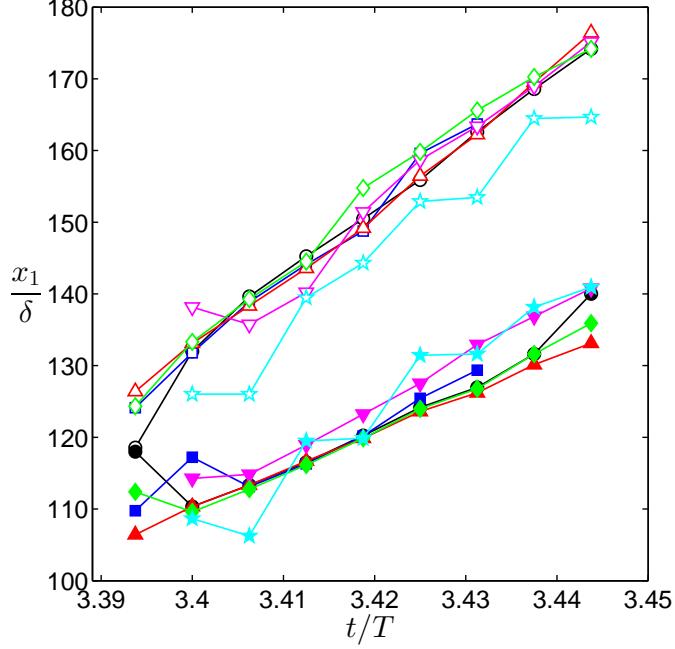


Figure 8: Evolution of the position of the head (open symbols) and tail (solid symbols) of the turbulent spot (the slope of the curves provides the velocity), obtained by considering different quantities to identify a turbulent spot: \star , $\star = \lambda_2$; \diamond , $\diamond = \text{TKE}$; \circ , $\bullet = \text{TKEP}$; \square , $\blacksquare = |u'_1|$; \triangle , $\blacktriangle = |u'_2|$; ∇ , $\blacktriangledown = |u'_3|$.

Table 1: Speed of the extremes of turbulent spots over a rough wall. u_{1H} , u_{1T} , u_{2L} and u_{2R} indicate the velocity of the head, tail, left-side and right side of the spots, respectively. The values in the first line are the result of the average over six spots. The results in the second line are by Carstensen et al. [2012] and refer to a single spot. The first column indicates the time interval during which turbulent spots are observed.

ωt (deg)	u_{1H}/U_0	u_{1H}/U_e	u_{1T}/U_0	u_{1T}/U_e	u_{2L}/U_0	u_{2L}/U_e	u_{2R}/U_0	u_{2R}/U_e
133-180	0.88	1.01	0.38	0.44	0.044	0.05	0.077	0.088
185-230	0.61	0.67	-	-	-	-	-	-

of the spots are reported in the first line of Table 1, both in terms of U_0 and in terms of the instantaneous free stream velocity $U_e(t)$. The measured values of the extreme points of the spot show a large variability from one spot to the other, particularly if the lateral sides are considered. Indeed, the smallest and largest values measured for the velocity of the right-side are $0.004 U_0$ and $0.194 U_0$, respectively, and those of the left-side are $0.022 U_0$ and $0.068 U_0$, respectively. As observed for spots forming over a smooth wall [Mazzuoli et al., 2011a], it is reasonable to expect, also in the present case, that similar values of the averaged speed of the left and right sides would be obtained if a larger statistical sample were considered.

The second line of Table 1 shows the values of the speed of the head of the turbulent spots measured by Carstensen et al. [2012]. It can be seen that Carstensen et al. [2012] measured a lower value for the speed of the head of the spots; moreover they observed the formation of turbulent spots at later phases of the cycle. The phases reported in Table 1 and in Table 2 are determined assuming that the external velocity is described by $U_e(t) = -U_0 \cos(\frac{2\pi}{T}t)$. Hence, the phases of the measurements by Carstensen et al. [2012], reported in Tables 1 and 2, show a 90° shift with respect to the original paper by Carstensen et al. [2012] because they considered the external velocity $U_e(t) = U_0 \sin(\frac{2\pi}{T}t)$.

It is possible to single out different causes for the differences in u_{1H} between Carstensen et al. [2012] and the present measurements. A possible reason might be the different geometry and equivalent roughness of the wall. Indeed, as already explained, the roughness used by Carstensen et al. [2012] was made with natural sand, while the numerical simulations were carried out by considering spherical roughness elements in a honeycomb arrangement. Moreover, as explained previously, the value of the equivalent sand roughness of the present case might deviate from that of the experiment by Carstensen et al. [2012].

A more convincing reason is related to the possible different distances from the wall at which the measurements and the numerical evaluations are performed. Indeed, Carstensen et al. [2012] identified turbulent spots by means of plan-view flow visualizations. In particular, they created a thin-layer of colored milk, of which they did not give the thickness, adhering to the bottom of their tunnel and interpreted the coherent structures made visible by the dye motion. On the other hand, we identified the turbulent spots on the plane $x_3 = 3.2\delta$, that corresponds to $x_3 = 5.63$ mm, i.e. 0.6 mm above the top of the spheres. To test the dependence of the measured characteristics of the spots on the selected plane, we computed the speed of the head of a spot also considering the plane $x_3 = 2.94\delta$ and we obtained $u_{1H} = 0.66U_0$, which is a value closer to that measured by Carstensen et al. [2012].

Another possible cause is due to the procedure used by Carstensen et al. [2012] to identify the contours of the spots, which they did not describe and

which presumably was based on the visual processing of the video frames of their movies. In order to test this hypothesis, we determined the speed of the head of the turbulent spot present in the rectangle in Fig. 4c, detecting by eye the position of the head on images of the streamwise velocity fluctuations, similar to those shown in Fig. 4. The obtained speed, averaged over 3 independent measurements, was $0.74 U_0$, a value smaller than that obtained by means of the numerical procedure, previously described.

Table 2: Speed of the extremes of turbulent spots over a smooth wall and time interval during which they were observed (second column). The data at $R_\delta = 775, 948, 1120$ are from Mazzuoli et al. [2011a] and those for $R_\delta = 777, 953$ are from Carstensen et al. [2012]. The phases of Mazzuoli et al. [2011a] are estimated on the basis of the values of U_e/U_0 .

R_δ	ωt	u_{1H}/U_0	u_{1H}/U_e	u_{1T}/U_0	u_{1T}/U_e	u_{2L}/U_0	u_{2L}/U_e	u_{2R}/U_0	u_{2R}/U_e
775	150	0.67	0.78	0.40	0.46	0.04	0.04	0.03	0.03
777	212-233	0.75	0.89	-	-	-	-	-	-
948	141	0.68	0.87	0.41	0.53	0.02	0.03	0.03	0.04
953	179-187	0.95	0.95	-	-	-	-	-	-
953	224-245	0.49	0.79	-	-	-	-	-	-
1120	123	0.51	0.94	0.33	0.61	0.02	0.04	0.03	0.05

In order to investigate the effect of the roughness of the wall on the speed of the turbulent spots, in Table 2 we report the values of the speed of the extreme points of the spots forming over a smooth wall, and available in the literature. In their experiments over a smooth wall, Carstensen et al. [2010] detected turbulent structures only for R_δ larger than 548. Investigations based on direct numerical simulations appear to confirm their experimental findings. Indeed Vittori and Verzicco [1998] showed that the flow over a smooth wall is in the intermittently turbulent regime only when R_δ exceeds 550, hence no turbulent spots are expected to form for lower values of R_δ . Mazzuoli et al. [2011a] conducted three simulations over a smooth wall at $R_\delta = 775, 948$ and 1220 and found that the speeds of the head and the tail of the turbulent spots, when expressed in terms of the phase-resolved free stream velocity $U_e(t)$, increases as R_δ is increased, while the speed of the sides of the spots do not show a significant dependence on R_δ .

Carstensen et al. [2012] observed turbulent spots over a rough wall for values of R_δ larger than 316. It is worthwhile to remark that a preliminary simulation did not show the formation of turbulent spots for $R_\delta=300$. Table 1 and 2 show that the speed of the head of the turbulent spots for the present simulation ($R_\delta = 400$) is larger than that measured over a smooth wall for the lowest values of R_δ available ($R_\delta=775, 777$ in Table 2). In order to compare the speed of the extreme points of the turbulent spots forming over a rough wall to those of turbulent spots forming over a smooth wall, let us consider the dependence, of u_{1H}/U_e and u_{1T}/U_e on R_δ in the

smooth wall case [Mazzuoli et al., 2011a]. Table 2 shows that in the smooth wall case u_{1T}/U_e increases as R_δ is increased. Assuming that a similar dependence of the speed of the head of the turbulent spots on R_δ holds also for the rough wall case, it could be argued that the effect of the roughness is that of increasing the speed of the head of the turbulent spots. Indeed the speed of the turbulent spots over the rough wall for $R_\delta = 400$ is larger than that of the turbulent spots that form over a smooth wall for larger values of R_δ . However, further numerical and experimental results would be necessary to determine the dependence of the speed of the head of the turbulent spots on both the roughness size and the Reynolds number. On the other hand, the speed of the tail and of the left side of the turbulent spot has similar values to the smooth wall case.

Considering the phases at which turbulent spots over a smooth wall form (see Table 2), it appears that during laboratory experiments by Carstensen et al. [2012] turbulent spots formed at later phases than in the numerical simulations by Mazzuoli et al. [2011a]. As discussed previously, a similar difference is found for turbulent spots forming over a rough wall, when comparing the experimental measurements Carstensen et al. [2012] with the present numerical results.

4 Conclusions

Transition to turbulence and the formation of turbulent spots in an oscillatory boundary layer are investigated and the average speed of the extreme points of these turbulent structures is determined. The boundary layer develops over a wall covered with spheres. The oscillatory boundary layer over a wall such as the one presently considered, can be laminar, transitional-turbulent or hydrodynamically-rough turbulent, depending on the values of R_δ and D/δ [Mazzuoli and Vittori, 2016]. For the values of R_δ and D/δ presently considered, the flow is in the transitional turbulent regime.

The present numerical investigation was inspired by one of the experiments by Carstensen et al. [2012] that observed the formation of turbulent spots over a rough wall and measured only the speed of the head of the turbulent spots. The present results allow a deeper understanding of transition in an oscillatory boundary layer over a rough wall. From the 3rd to the 5th half oscillation cycle, during the accelerating phases, only transverse vortices with a marked periodicity are observed. As the flow decelerates, the transverse vortices dissipate. After the 5th half cycle, high- and low-speed streaks form close to the wall and are subject to an evolution similar to that which is observed on a smooth wall [Vittori and Verzicco, 1998, Costamagna et al., 2003]. Also the spacing of the streaks is similar to that of the streaks observed over a smooth wall [Costamagna et al., 2003].

Starting from the 6th half oscillation cycle (last part of the 3rd cycle),

during the late accelerating phase, the interaction of low- and high-speed streaks with weak vorticity, which survived from the previous half-cycle, gives rise to turbulent spots, following a by-pass transition mechanism.

The speed of the head of the turbulent spots is slightly larger than that measured by Carstensen et al. [2012]. The discrepancy can be explained considering that it was not possible to reproduce exactly the experimental conditions and in particular the wall geometry, which was covered with natural sand grains in Carstensen et al. [2012]. Small quantitative differences between experimental measurements and numerical results should not be surprising, also because of the different approach used to detect and measure the turbulent spots. The comparison of the speed of the extreme points with that of the smooth wall case [Mazzuoli et al., 2011a] *suggests* that the speed of the head of the turbulent spots over the rough wall is larger than that over the smooth wall, while that of the tail and of the lateral points has similar values.

We measured the characteristics of turbulent spots, averaged over six spots, only for one value of the Reynolds number and for one roughness size. However, present investigation has allowed to highlight the mixed (natural/bypass) path of this flow from the laminar regime to turbulence. In order to reach definitive conclusions on the effect of the wall roughness on the characteristics of the turbulent spots, it would be necessary to consider different values of R_δ and D/δ , such that the flow regime falls also in the hydrodynamically rough turbulent regime. Such simulations are currently at the limit of the present supercomputing capabilities as they require a large amount of computational resources (the simulation with $R_\delta=400$ and $D/\delta=2.8$ used approximately 8M core hours in the supercomputer FERMI, CINECA).

5 Acknowledgments

The Authors thank Markus Uhlmann for providing the code used in the present research. The computer time for the numerical experiments was provided by CINECA (Bologna, Italy) under grant TEST SEA (PRACE 7th-call). The computational resources for the post processing of the data was jointly provided by CINECA (ISCRA Project TESTSEAP - HP10CA8L71) and by Steinbuch Center for Computing (KIT, Karlsruhe).

References

- R. Akhavan, R. D. Kamm, and A. H. Shapiro. An investigation of transition to turbulence in bounded oscillatory stokes flows part 1. experiments. *Journal of Fluid Mechanics*, 225:395422, 1991. doi: 10.1017/S0022112091002100.

- P. Blondeaux and G. Vittori. Wall imperfections as a triggering mechanism for stokes-layer transition. *Journal of Fluid Mechanics*, 264:107–135, 1994.
- S. Carstensen, B. M. Sumer, and J. Fredsøe. Coherent structures in wave boundary layers. part 1. oscillatory motion. *Journal of Fluid Mechanics*, 646:169–206, 2010.
- S. Carstensen, B. M. Sumer, and J. Fredsøe. A note on turbulent spots over a rough bed in wave boundary layers. *Physics of Fluids*, 24(11):115104, 2012.
- P. Costamagna, G. Vittori, and P. Blondeaux. Coherent structures in oscillatory boundary layers. *Journal of Fluid Mechanics*, 474:1–33, 2003.
- M. Detert, V. Nikora, and G.H. Jirka. Synoptic velocity and pressure fields at the water–sediment interface of streambeds. *Journal of Fluid Mechanics*, 660:55–86, 2010.
- H. W. Emmons. The laminar-turbulent transition in a boundary layerpart i. *J. aeronaut. Sci*, 18(7):490–498, 1951.
- F. Fornarelli and G. Vittori. Oscillatory boundary layer close to a rough wall. *European Journal of Mechanics-B/Fluids*, 28(2):283–295, 2009.
- C. D. Ghodke and S. V. Apte. Dns study of particle-bed–turbulence interactions in an oscillatory wall-bounded flow. *Journal of Fluid Mechanics*, 792:232–251, 2016.
- B. L. Jensen, B. M. Sumer, and J. Fredse. Turbulent oscillatory boundary layers at high reynolds numbers. *Journal of Fluid Mechanics*, 206:265297, 1989. doi: 10.1017/S0022112089002302.
- J. Jeong and F. Hussain. On the identification of a vortex. *Journal of fluid mechanics*, 285:69–94, 1995.
- P.M. Ligrani and R.J. Moffat. Structure of transitionally rough and fully rough turbulent boundary layers. *Journal of Fluid Mechanics*, 162:69–98, 1986.
- M. Mazzuoli and M. Uhlmann. Direct numerical simulation of open-channel flow over a fully rough wall at moderate relative submergence. *Journal of Fluid Mechanics*, 824:722765, 2017. doi: 10.1017/jfm.2017.371.
- M. Mazzuoli and G. Vittori. Transition to turbulence in an oscillatory flow over a rough wall. *Journal of Fluid Mechanics*, 792:67–97, 2016.
- M. Mazzuoli, G. Vittori, and P. Blondeaux. Turbulent spots in oscillatory boundary layers. *Journal of Fluid Mechanics*, 685:365–376, 2011a.

- M Mazzuoli, G Vittori, and P Blondeaux. Turbulent spots in a stokes boundary layer. *Journal of Physics: Conference Series*, 318(3):032032, 2011b. URL <http://stacks.iop.org/1742-6596/318/i=3/a=032032>.
- M.M. Pimenta, R.J. Moffat, and W.M. Kays. The turbulent boundary layer: an experimental study of the transport of momentum and heat with the effect of roughness. Technical report, STANFORD UNIV CA THERMO-SCIENCES DIV, 1975.
- H. Schlichting and K. Gersten. *Boundary-layer theory*. Springer, 2016.
- G. B. Schubauer and P. S. Klebanoff. Contributions to the mechanics of boundary-layer transition naca tn-3489. Technical report, Washing, United States, 1955.
- K.M. Singh, N.D. Sandham, and J.J.R. Williams. Numerical simulation of flow over a rough bed. *Journal of Hydraulic Engineering*, 133(4):386–398, 2007.
- M. Uhlmann. An immersed boundary method with direct forcing for the simulation of particulate flows. *Journal of Computational Physics*, 209(2):448–476, 2005.
- G. Vittori and R. Verzicco. Direct simulation of transition in an oscillatory boundary layer. *Journal of Fluid Mechanics*, 371:207–232, 1998.